Automated dynamic motion correction using normalized gradient fields for ^{82}rubidium PET myocardial blood flow quantification

Supplemental Materials

Benjamin C. Lee, PhD[1]; Jonathan B. Moody, PhD[1]; Alexis Poitrasson-Rivière, PhD[1]; Amanda C. Melvin, MS[2]; Richard L. Weinberg, MD, PhD[3]; James R. Corbett, MD[1,2]; Venkatesh L. Murthy, MD, PhD[2 *]; Edward P. Ficaro, PhD[1,2 *]

1. INVIA Medical Imaging Solutions, Ann Arbor, MI
2. Division of Nuclear Medicine, Department of Radiology, University of Michigan, Ann Arbor, MI
3. Division of Cardiovascular Medicine, Department of Internal Medicine, University of Michigan, Ann Arbor, MI
(* Dr. Ficaro and Dr. Murthy contributed equally to this work and are co-senior authors)

Supplemental Results

Automated Motion-Correction Extended Case Study

Supplemental Figure 1 illustrates the effectiveness of the automated motion-correction algorithm applied to two additional representative dynamic frames of a dynamic PET sequence. Supplemental Figure 1C highlight the 2 representative frames with their similarity score weights for the RVBP, LVBP, and tissue.

In frame 8 which starts at 35 seconds, the tracer activity was transitioning from the LVBP to the tissue with roughly equal activity (Supplemental Figure 1D). The uncorrected frame had a weighted similarity score of 5: 30% of RVBP score of -1 (not shown), 36% of the LVBP score of 0 (Supplemental Figure 1F), and 35% of the tissue score of 16 (Supplemental Figure 1G). The corrected transition NGF (Supplemental Figure 1I) had a weighted similarity score of 7: 30% of RVBP score of -1 (not shown), 36% of the LVBP score of 1 (Supplemental Figure 1J), and 35% of the tissue score of 18 (Supplemental Figure 1K). Similarity was greatest in the epicardial edge surface in the tissue similarity map. While the LVBP similarity map showed a moderate match in the endocardial edge surface it was cancelled out by the nearly equally opposite penalty values in the tissue similarity map.

In frame 26 which starts at 200 seconds, the tracer activity had mostly been taken up by the tissue (Supplemental Figure 1L). The uncorrected frame had a weighted similarity score of 20: 13% of RVBP score of -1 (not shown), 14% of the LVBP score of -3 (Supplemental Figure 1N), and 73% of the tissue score of 28 (Supplemental Figure 1O). Due to zero estimated motion shifts, the corrected frame was unchanged and had the same weighted similarity score of 20. Similarity was already greatest both in the epicardial and endocardial

edge surfaces in the tissue similarity map. The LVBP VOI is mismatched in Supplemental Figure 1N but its score was outweighed five-fold by the tissue score, as expected since the activity mostly cleared the LVBP.

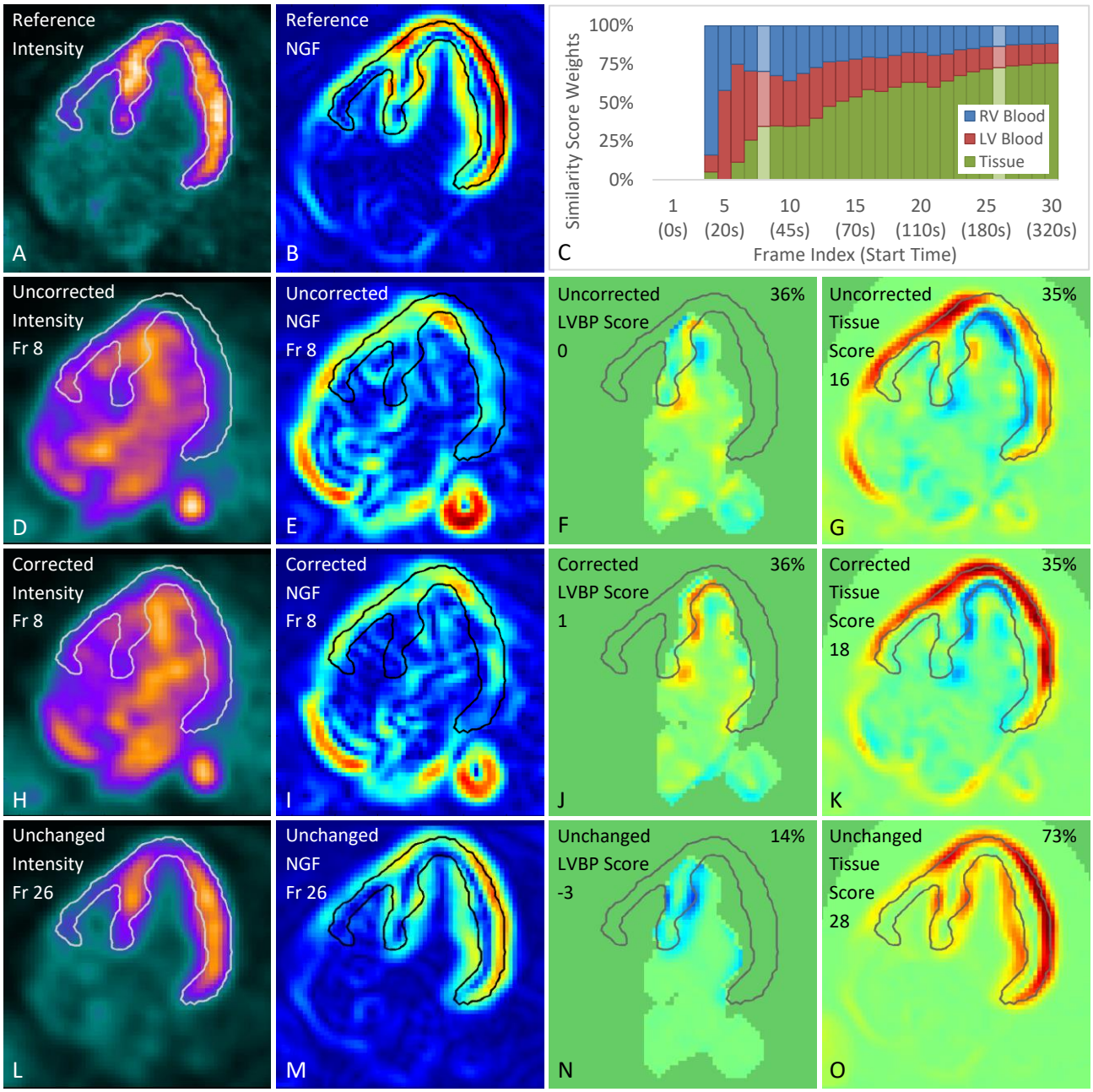

Supplemental Figure 1. Automated motion correction example in the (D-K) transition and (L-O) tissue phase with (A-B) reference image volume and (C) similarity score weights. Similarity scores vary from high (red) to low (blue). The frames selected are highlighted (lighter shade) in the similarity score weights plot (C). *NGF* indicates normalized gradient field; *Fr*, frame; *LV*, left ventricle; *RV*, right ventricle; *LVBP*, left ventricular blood pool.

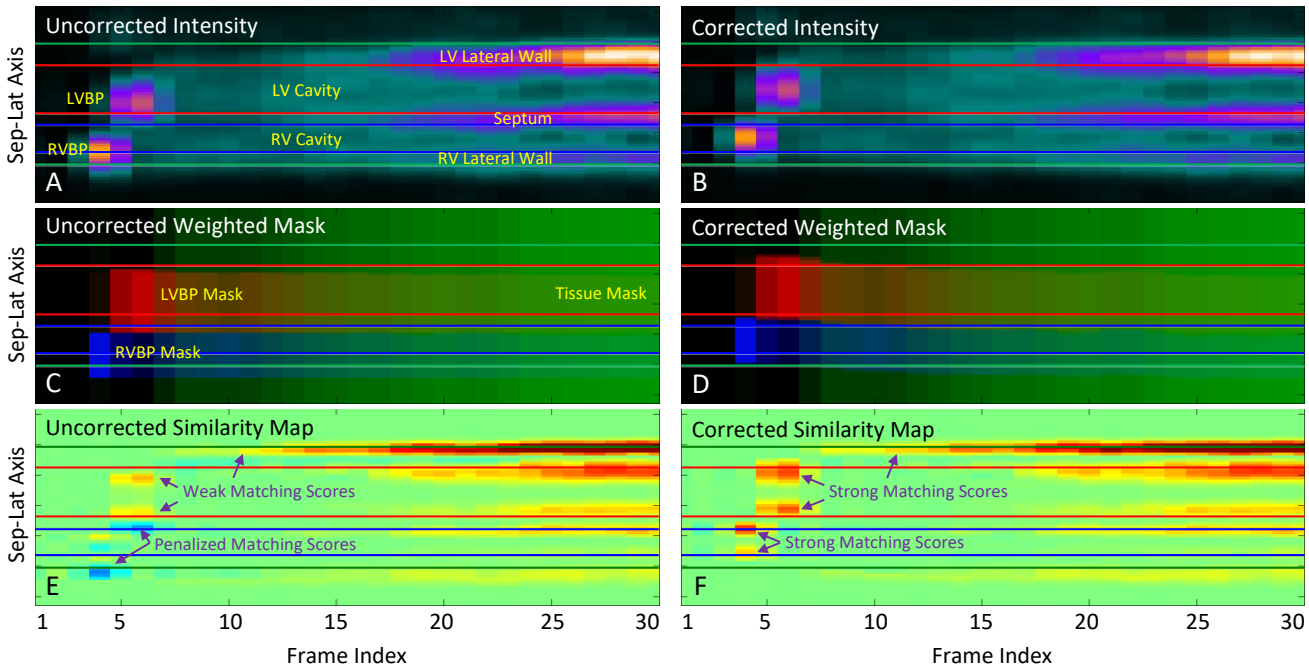

Supplemental Figure 2. Automated motion correction example shown in spatial (vertical) and temporal (horizontal) axes, where the spatial axis is in the septal-lateral direction and fixed in the mid-apical-basal and mid-inferior-anterior slices. Overlaid horizontal lines indicate the edge surface estimates of the LV lateral and RV epicardial contours (green), LV endocardial contours (red), and RV endocardial contours (blue). (A, B) Intensities show hot activity in the early frames of the blood phase then decrease in the later tissue phase. (C, D) Weighted masks show the blood pool isolate algorithm localized the right ventricular blood pool (blue), the left ventricular blood pool (red), and the tissue (green), with the associated similarity weights denoted by color brightness. (E, F) Similarity maps show in space and time, matches between the moving frame and the reference with high (red) and low (blue) similarity scores. (A, C, E) Uncorrected dynamic sequences show grossly misaligned blood pool activity, masks, and scores in the early frames and less misaligned tissue activity in the later frames. (B, D, F) Automated motion-corrected sequences show properly aligned activity, masks, and scores across all frames. *Sep* indicates septal; *Lat*, lateral; *LV*, left ventricle; *RV*, right ventricle; *LVBP*, left ventricular blood pool; *RVBP*, right ventricular blood pool.

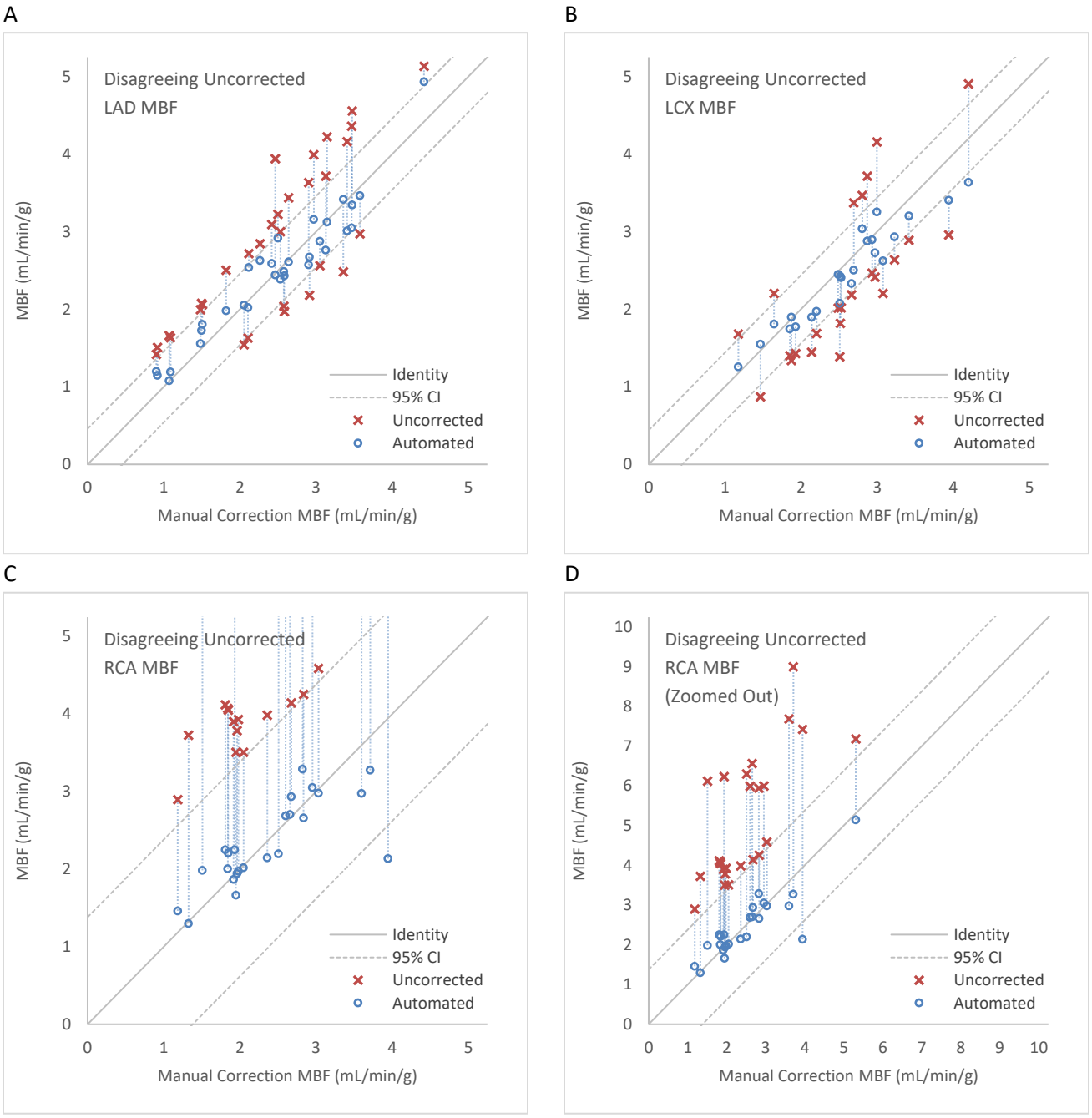

Supplemental Figure 3. Automated motion-correction effects on **regional** MBF in the (A) LAD, (B) LCX, and (C, D) RCA vascular territories. Uncorrected flows with differences outside of the limits of agreement (95% confidence intervals) with manual-correction flows improve after automated correction, indicated by connecting vertical lines, falling within the same limits of agreement in all but one LAD, four LCX, and one RCA cases. Eleven high flow values above 5 $mL \cdot min^{-1} \cdot g^{-1}$ from the RCA territory that are not shown in (C) are shown in the same plot with wider axes limits in (D).

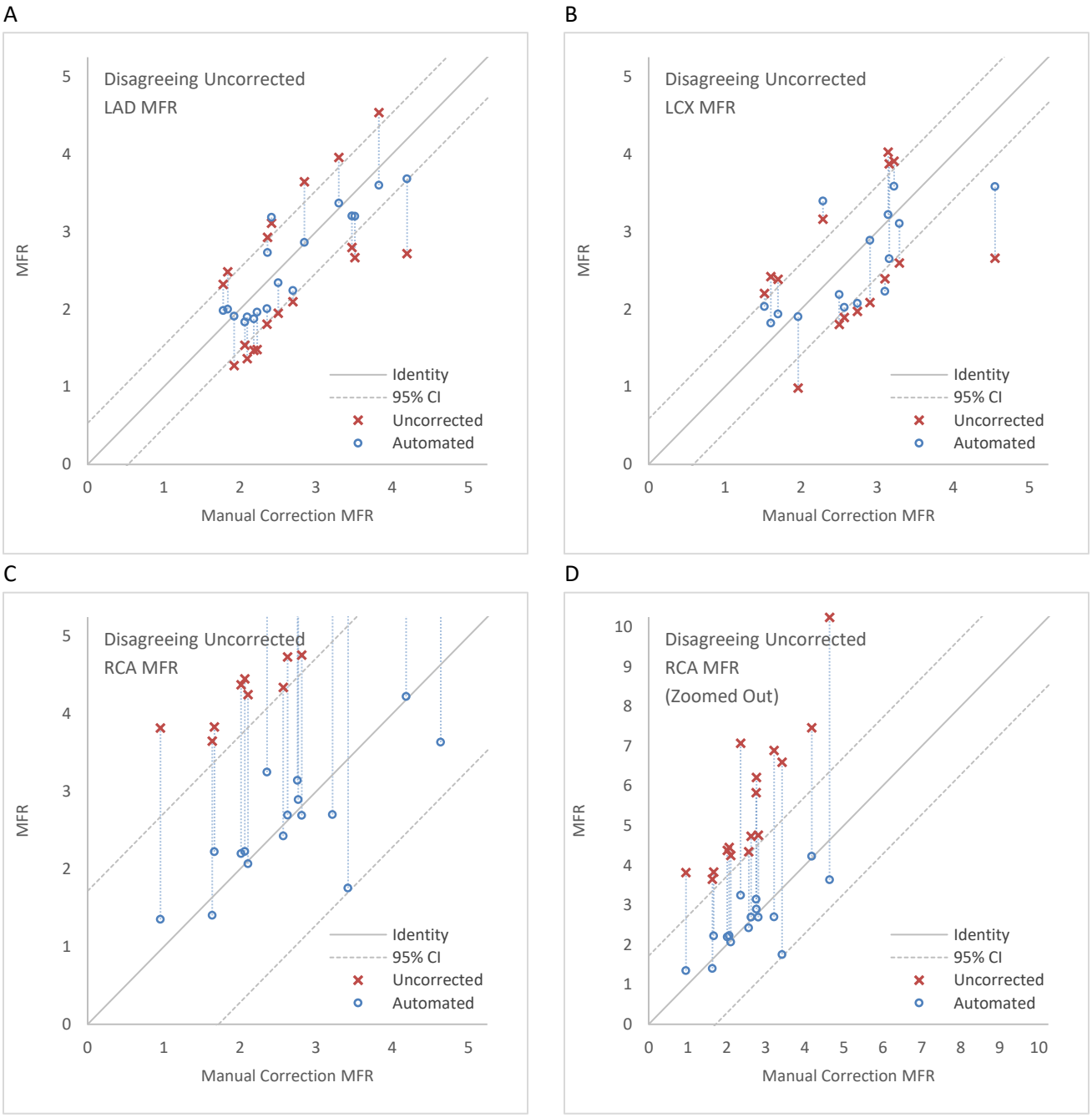

Supplemental Figure 4. Automated motion-correction effects on **regional** MFR in the (A) LAD, (B) LCX, and (C, D) RCA vascular territories. Uncorrected reserve values with differences outside of the limits of agreement (95% confidence intervals) with manual-correction reserve values improve after automated correction, indicated by connecting vertical lines, falling within the same limits of agreement in all but one LAD, four LCX, and zero RCA cases. Seven high reserve values above 5 from the RCA territory that are not shown in (C) are shown in the same plot with wider axes limits in (D).

Supplemental Discussion

Comparison to Alternative Image Registration Algorithms

We and others have previously attempted motion correction by attempting to minimize the distance between LV blood and tissue surfaces. These feature-based image registration methods have disadvantages of inaccurate surface estimation and not utilizing all the information in the image volume. Some of these estimated surfaces without strong edges are often interpolated and smoothed, introducing bias and then drawing influence away from the correct edges. Intensity-based image registration algorithms utilize information that may have otherwise been discarded by a feature-based algorithm. Some examples in cardiac imaging of information discarded by feature-based algorithms that are used by our approach include: (1) the interface between the base of the septal wall and the left ventricular outflow tract and (2) the influence of papillary muscles on the shape of the endocardial surface.

Automated motion estimation of the tissue-phase frames matched against a similar tissue weighted-average reference image volume has been studied extensively in the field of image registration by finding similarities in image intensities. However, the motion estimation of the blood phase required matching complementary but albeit dissimilar image volumes. Reframing this problem of matching blood-phase image volumes with tissue-phase image volumes as multi-modal image registration opens up powerful methods such as mutual information and normalized mutual information.[1–3] However, there are many disadvantages to mutual information which include difficulty in finding a global solution and a failure to use spatial information associated with each voxel intensity.[4,5] Normalized gradient fields are also suited for multi-modal image registration and can better estimate global solutions and utilize the spatial information of each voxel through the calculation of normalized gradients from its neighbors. In the study using dynamic contrast enhanced MRI to model kidney dynamics, NGFs were found to perform better than mutual information with smoother TACs leading to lower compartmental modeling uncertainty.[6]

Blood Pool Isolation

While the tissue phase frames required gradients in the same direction as the reference weighted-average tissue image volume, the blood-phase frames required gradients in the opposite direction as the reference image volume. The nonoverlapping RVBP and LVBP VOIs further required the RVBP image volume to be subtracted from the LVBP image volume. In prior work, a factor analysis algorithm was applied to cardiac dynamic images to generate RVBP, LVBP, and tissue TACs and their associated factored images.[7,8] Yet with added knowledge of approximate location of the RVBP and LVBP with respect to the known LV myocardium and their sequence of peak activities in time, our novel blood pool isolation algorithm estimated the RVBP and LVBP with significantly less computation (<0.1 seconds per case) than factor analysis methods (~110 seconds per case), enabling rapid spatio-temporal localization of the tracer activity in preparation for automated motion correction.

Normalized Gradient Fields and Modification Details

The formulation in this study, using multiple similarity measures customized to each phase of the dynamic sequence and where the similarity measure retains the sign of the gradient, differs from the conventional NGF similarity score, which is a sum of squared dot products. The modified formulation used in this study distinguishes matches between gradients in the same direction from mismatches between gradients in opposite

directions, which serve as a penalty and improves the accuracy of matches. For example, using a sum of squares does not distinguish the matching of two endocardial surfaces and matching of an endocardial surface with an epicardial surface. If the moving frame was from the tissue phase, it was expected to have many matching gradients with the reference image volume, which was computed from the tissue frames. If the moving frame was from one of the blood pool phases, it was expected to have fewer matching gradients with the reference image volume. In this case, the modified formulation favors matches between gradients in opposite directions and penalizes mismatches of gradients in the same direction. A falling edge at the surface of the blood pool and the rising edge of the endocardial surface have gradients in opposite directions but are expected to match, whereas the surface of the blood pool and the epicardial surface have gradients in the same direction but are not expected to match. Throughout the dynamic sequence, in many cases, the blood pool does not completely clear in the tissue phase or the RVBP and LVBP activities overlap with each other. Combining the three similarity measures using time-dependent weights based on their relative signal strengths in the form of TACs allows for smoother motion estimation and a decomposition of ambiguous activity into fundamental components as in the transition frames. The spatial bounding masks used for the computation of the similarity measures also reduced the number of computations which led to faster automated motion-correction run-times of 14 seconds per study or 7 seconds per dynamics sequence or 0.2 seconds per temporal frame.

Supplemental References

1. Viola P, Wells III WM. Alignment by Maximization of Mutual Information. *Int J Comput Vis*. 1997;24(2):137–154. doi:https://doi.org/10.1023/A:1007958904918.

2. Maes F, Collignon A, Vandermeulen D, Marchal G, Suetens P. Multimodality image registration by maximization of mutual information. *IEEE Trans Med Imaging*. 1997;16(2):187-198. doi:10.1109/42.563664.

3. Studholme C, Hill DLG, Hawkes DJ. An overlap invariant entropy measure of 3D medical image alignment. *Pattern Recognit*. 1999;32(1):71-86. doi:10.1016/S0031-3203(98)00091-0.

4. Haber E, Modersitzki J. Intensity gradient based registration and fusion of multi-modal images. *Methods Inf Med*. 2007;46(3):292-299. doi:10.1160/ME9046.

5. Pluim JPW, Maintz JBA, Viergever MA. Mutual-information-based registration of medical images: a survey. *IEEE Trans Med Imaging*. 2003;22(8):986-1004. doi:10.1109/TMI.2003.815867.

6. Hodneland E, Lundervold A, Rørvik J, Munthe-Kaas AZ. Normalized gradient fields for nonlinear motion correction of DCE-MRI time series. *Comput Med Imaging Graph Off J Comput Med Imaging Soc*. 2014;38(3):202-210. doi:10.1016/j.compmedimag.2013.12.007.

7. Sitek A, Di Bella EV, Gullberg GT. Factor analysis with a priori knowledge--application in dynamic cardiac SPECT. *Phys Med Biol*. 2000;45(9):2619-2638.

8. El Fakhri G, Sitek A, Guérin B, Kijewski MF, Di Carli MF, Moore SC. Quantitative dynamic cardiac 82Rb PET using generalized factor and compartment analyses. *J Nucl Med Off Publ Soc Nucl Med*. 2005;46(8):1264-1271.